Vibrational Motions Associated with Primary Processes in Bacteriorhodopsin Studied by Coherent Infrared Emission Spectroscopy

Géza I. Groma,[†‡*] Anne Colonna,[†] Jean-Louis Martin,[†] and Marten H. Vos[†]

[†]Laboratory for Optical Biosciences, Ecole Polytechnique, Institut National de la Santé et de la Recherche Médicale, Centre National de la Recherche Scientifique, Palaiseau, France; and [‡]Institute of Biophysics, Biological Research Centre, Hungarian Academy of Sciences, Szeged, Hungary

ABSTRACT   The primary energetic processes driving the functional proton pump of bacteriorhodopsin take place in the form of complex molecular dynamic events after excitation of the retinal chromophore into the Franck-Condon state. These early events include a strong electronic polarization, skeletal stretching, and all-*trans*-to-13-*cis* isomerization upon formation of the J intermediate. The effectiveness of the photoreaction is ensured by a conical intersection between the electronic excited and ground states, providing highly nonadiabatic coupling to nuclear motions. Here, we study real-time vibrational coherences associated with these motions by analyzing light-induced infrared emission from oriented purple membranes in the 750–1400 cm^{-1} region. The experimental technique applied is based on second-order femtosecond difference frequency generation on macroscopically ordered samples that also yield information on phase and direction of the underlying motions. Concerted use of several analysis methods resulted in the isolation and characterization of seven different vibrational modes, assigned as C-C stretches, out-of-plane methyl rocks, and hydrogen out-of-plane wags, whereas no in-plane H rock was found. Based on their lifetimes and several other criteria, we deduce that the majority of the observed modes take place on the potential energy surface of the excited electronic state. In particular, the direction sensitivity provides experimental evidence for large intermediate distortions of the retinal plane during the excited-state isomerization process.

INTRODUCTION

Retinal proteins are of high importance in a wide range of living organisms. They are involved both in visual perception of vertebrates and many invertebrates and in light-energy transduction of an increasingly documented class of underwater microorganisms (1,2). The best studied retinal protein utilizing light energy is bacteriorhodopsin (bR). bR builds up a transmembrane potential by a proton-pumping mechanism during its photocycle initiated by light absorption (3,4). The early steps of this photocycle can be briefly summarized in terms of intermediates distinguished by visual absorption spectroscopy as (5–8):

$$bR_{568} \xrightarrow{h\nu} FC \xrightarrow{200fs} I_{460} \xrightarrow{500fs} J_{625} \xrightarrow{3ps} K_{610}.$$
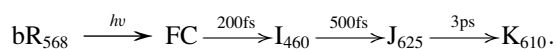
Here, bR_{568} denotes the electronic ground state (S_0) of the resting form of bR, FC and I_{460} correspond to the Franck-Condon and the energetically minimum structures of the first electronically excited state (S_1), respectively, and J_{625} and K_{610} are the two first ground-state intermediates of the photocycle. It is evident from extensive experimental data that the configuration of the retinal chromophore is all-*trans* in the bR_{568} form and 13-*cis* in the K_{610} intermediate (8–13). However, the detailed timing of the isomerization and its interplay with other ultrafast processes are still subjects of intense debate.

Early time-resolved transient absorption experiments (14,15) resulted in an initially widely accepted model proposing molecular motion on the excited-state potential energy surface (PES) along a single degree of freedom, the torsion around the $C_{13}=C_{14}$ bond, directly coupled to the optical transition. A more advanced description of the photoprocesses of retinal is based on the concept of a multidimensional conical intersection (CI). Here, beyond the torsional motion, at least one additional reaction coordinate is required, and the PESs are described as hypersurfaces that experience strong nonadiabatic coupling at true crossing points, or even seams, allowing the photoreaction to be funneled at a very high rate, efficiency, and selectivity (16,17). Ab initio quantum chemical simulations indicated that the relaxation of the S_1 state can be described as a two-mode molecular motion: initial relaxation from the FC region is dominated by skeletal stretching, and the CI is formed by coupling this reaction path to the isomerization process (18–20). Unlike S_0, which has a covalent A_g-like (dot-dot) character, S_1 has a highly ionic B_u-like (hole-pair) structure (19). The corresponding positive charge transfer along the hydrocarbon tail upon excitation to the FC region is known as sudden polarization, from early literature (21–23) speculating about the functional role of this effect in the energy-transduction process. The charge-transfer nature of S_1 is maintained, and even increased, during the two-mode pathway of relaxation (19,20,24). Altogether, isomerization through a CI cannot be handled as a separate event, because it is intertwined with other major processes such as intramolecular charge transfer and skeletal stretching.

Recent hybrid ab initio quantum mechanical/molecular mechanical (QM/MM) calculations made possible a detailed

*Correspondence: groma@brc.hu

Editor: Leonid S Brown.

characterization of the excited-state dynamics of both isolated and protein-bound retinal (24–27). These calculations highlighted the modulation of the energy difference between S_1 and S_0 by vibrational modes corresponding to $C_{13}=C_{14}$ and $C_{15}=N$ stretching, hydrogen-out-of-plane (HOOP) wagging, and in-plane rocking, as well as by $C_{13}=C_{14}$ torsional rocking modes. These theoretical results are in good agreement with numerous experimental observations of coherent vibrations coupled to ultrafast absorption end stimulated emission kinetics of bR (7,12,28–34). The direct assignment to S_1 or S_0 of the different vibrational modes obtained by these experiments, however, is not trivial, since ground-state coherent vibrations also can be excited by the pump pulse via the process of resonant impulsive stimulated Raman scattering (RISRS) (29,32,35,36).

Conventional frequency-domain spectroscopy was extensively applied to characterize the resting state of bR (37), as well as the different photointermediates, including static resonance Raman (9) and infrared (IR) (38,39) studies on the K form stabilized at 77 K. Developments in both experimental techniques made it possible to follow the time evolution of the bR vibrational modes in the picosecond (10,11,40–42) and femtosecond (8,13,43,44) domains. The majority of time-resolved resonance Raman and IR absorption experiments supports the view that the chromophore in J is already in 13-*cis*, although the final planar form of that isomer is achieved only in the K state (8,10,13). In accordance with the theoretical results summarized above, C=C and C-C stretching modes were observed preceding the isomerization (8,40,43), as was increased activity of HOOP modes in the J and K intermediates (8,10,11,41).

Coherent detection of the electromagnetic emission related to light-induced polarization changes of the chromophore is an alternative to follow the time evolution of retinal vibrational modes. This method, based on a molecular Hertzian dipole radiation, was first applied in the characterization of vibrational coherences of myoglobin (45), then in the study of light-induced charge-translocation processes in bR, in both the mid-IR (46,47) and the terahertz (48) domains. Our time-domain mid-IR emission experiments revealed that this ultrafast electronic polarization of retinal appears in <~10 fs, as manifested by a resonant optical rectification signal (46), and allowed the determination of its magnitude (47). Detecting the emission in a lower frequency range by the methods of terahertz spectroscopy (48) made it possible to follow the decay of this excited-state polarization, as well as the emergence of the first component of the functional proton pump of bR. Beyond these rectified charge-translocation processes, the high time resolution of the mid-IR technique also made it possible to visualize coherent vibrational motions, corresponding in principle to all IR-active modes of the retinal/protein system in the detection window set in motion directly or indirectly by light absorption of the retinal (46). Activation of vibration coherences in both the ground

and excited electronic states by a short pump pulse of resonant wavelength on a noncentrosymmetric sample can be described by the theory of difference-frequency generation (49). As macroscopically oriented samples are used, in principle, directional information also can be retrieved. The method requires an initial resonant excitation of the sample that quasi-instantaneously generates an off-equilibrium excited state, but detection of the ensuing vibrations does not require direct coupling to any electronic transition. In this context, it is complementary to techniques detecting coherent modulations of absorption kinetics and transient (stimulated) Raman spectroscopy that specifically monitor vibrations directly coupled to such transitions. The goal of this article is to characterize in detail the coherences detected by coherent emission from bR in experiments. The concept of the coherent IR emission measuring technique (45,46) is demonstrated in Fig. S1 in the Supporting Material.

MATERIALS AND METHODS

Sample preparation

Purple membranes from *Halobacterium salinarum* were prepared by the standard method (50). Dried oriented neutral bR films were prepared through electrophoretic deposition of membrane suspensions on germanium plates followed by drying under ~50% relative humidity (51). These films had a thickness of ~10 μm and an optical density of ~2 at the 568-nm visible absorption maximum. Acid blue samples were obtained by immersion of dry samples in H_2SO_4 solutions for a few minutes and subsequent redrying (52,53). In both types of film the initial photoinduced events in the photocycle have been shown to be unaltered with respect to those in the aqueous environment (52).

Experimental apparatus

The experimental setup used for the coherent infrared bR emission was described in detail previously (45,46). Briefly, the output of a noncollinear parametric amplifier, centered at 560 nm, with 11-fs pulse duration and ~90-nm spectral half-width, was split into two beams. One beam was used to excite the bR films, which emitted in the IR through light-induced intramolecular polarization processes. The angle between the plane perpendicular to the beams and the normal axis of the film was set at 45° to collect maximum IR emission. The sample was continuously rotated in the plane of the film to avoid excitation of photointermediates that are relatively long-lived in dried bR (52,54). The other beam was focused on a GaAs sample, which also emitted in the IR through electronic optical rectification. This single-cycle IR emission was used as a reference beam for interferometric heterodyne detection. In this study, GaAs was applied as a reference material, because it has higher net conversion efficiency than $AgGaS_2$ and therefore a higher signal/noise ratio in the interferograms is possible (47). The two IR beams were focused and spatially overlapped on an HgCdTe detector, and an interferogram was constructed by varying the time delay between the beams in 4-fs steps.

The transfer function of the measuring apparatus, $T(t)$, was determined by an $AgGaS_2$ sample. The emission from this transparent, non-phase-matching, nonlinear material is also due to optical rectification, and its temporal response to a short visible pulse can be well described as following the envelope of the pump pulse (47). Hence the transfer function was obtained from the deconvolution of the corresponding interferogram with that envelope in the frequency domain, supposing a Gaussian pulse

shape of 11 fs full width at half-maximum (FWHM). This procedure was performed with the bR sample in the IR beam to include its filtering effect.

Data analysis

The spectrogram of the measured interferograms, based on sliding-window Fourier analysis, was calculated by the Signal Processing Toolbox of MAT-LAB (The MathWorks, Natick, MA). As a reasonable tradeoff between temporal and spectral resolution, in most analyses, a Hann (Hanning) window (55) of 100 points (corresponding to a 400-fs length and 200-fs FWHM) was applied.

In a complementary approach, the interferograms were fitted by a nonlinear least-square procedure in the framework of a model supposing IR radiation of bR by an electronic (optical rectification) and a multimodal vibrational process. The resonant optical-rectification component was described by the first time derivative of the electronic polarization, modeled by an instantaneous rise and a 500-fs decay time of the excited state (45,46). The ith component of the damped vibrational modes was expressed as $A_i\exp(-t/\tau_i)\cos(\omega_i t + \varphi_i)$ (45), with positivity constraint on A_i (i.e., controlling the sign of a component by φ_i). The complete fitting model was obtained by convolution of this molecular response with the envelope of the pump pulse and $T(t)$. The relative amplitude of the electronic response, as well as A_i, τ_i, ω_i, and φ_i, were free fitting parameters. Since the electronic part of the interferogram highly outweighs the vibrational one (Fig. 1), small uncertainties in the modeling of the former may lead to high errors in the parameters of the latter, which was the main interest of this study. To avoid this problem, we temporally separated the two components and applied different weights on them in the fitting procedure. First, the zero delay, t_0, was estimated from the maximum of the signal, then the $t < 160$ fs section of the interferogram was fitted with a high (50:1) weight, taking the electronic process into account predominantly, to determine the exact value of t_0. In a second step, the high weight was given to the section of $t \geq 160$ fs, the value of t_0 was kept fixed, and the complete response model was applied. The average values of the fitting parameters listed in Tables 1 and 2 were obtained from three independent measurements.

The power spectrum estimation of the $t \geq 160$ fs section of the interferograms was calculated by the Yule-Walker autoregressive method (56), implemented in the Signal Processing Toolbox of MATLAB using an order parameter of 250. The spectral response of the measuring system was obtained by the Fourier transform of $T(t)$ (see Fig. 4).

For comparison of the different measurements, all interferograms were normalized to the maximum of their electronic part before further analysis.
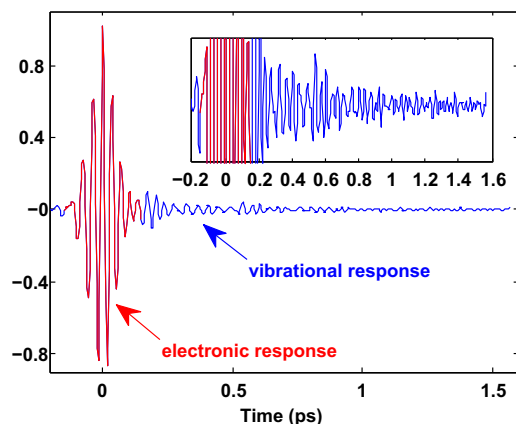

FIGURE 1   Interferogram between the IR emissions from native bR and GaAs reference. The interferogram shows two parts, the instantaneous electronic response around zero delay time and a signal at positive time that reflects vibrational motions of the retinal/protein system. (*Inset*) Amplitude enlargement (20×) of the interferogram.

TABLE 1   Fitting parameters of the vibrations of native bR

Mode ID	Frequency* (cm^{-1})	Phase† (°)	Decay time‡ (fs)	Amplitude§ (relative)
M1	773	−169	>2000	0.015
M2	856	161	860	0.057
M3	910	−165	230	0.25
M4	989	−18	260	1.0
M5	1056	−15	600	0.079
M6	1110	−35	>2000	0.016
M7	1184	−136	410	0.9

The fitting procedure localized the frequencies well, whereas the uncertainties of the other fitting parameters were relatively large due to their high number and the limitations of the model. Typical error values of the parameters are noted.
*The typical frequency error was 15 cm^{-1}.
†The typical phase error was 60°.
‡The typical decay-time error was 230 fs.
§The typical amplitude error was 40%.

RESULTS

Fig. 1 shows the light-induced coherent IR emission from a native, dried oriented bR sample interfering with the single-cycle reference IR pulse emitted by a GaAs crystal. The dominant feature of the interferogram is the electronic response around zero delay time (46), with extensive side lobes caused by the low-frequency cut-off of the detector (45). However, the interferogram is asymmetric, with long-lived oscillations in the range $t > 150$ fs, reflecting coherent vibrations of IR-active modes (45). In the sliding-window spectrogram (Fig. 2), the electronic response is represented by a high-intensity (*red*) area near $t = 0$, distributed over the whole 650–1600 cm^{-1} spectral range where the technique is sensitive (45). The long-lived oscillations occur mainly in the 750–1400 cm^{-1} region. This region shows a complex structure with contributions from multiple damped vibrational modes. Parts of the spectrogram are indicative of time-dependent frequencies (e.g., Fig. 2, region A), and apparent recurrences (Fig. 2, region B). These features may represent real phenomena (7,12,32–34), i.e., anharmonicities of the potential energy surfaces and/or frequency changes between different electronic states, but they also can be partially due to the beating of the different modes. Fig. 2

TABLE 2   Fitting parameters of the vibrations of acid blue bR

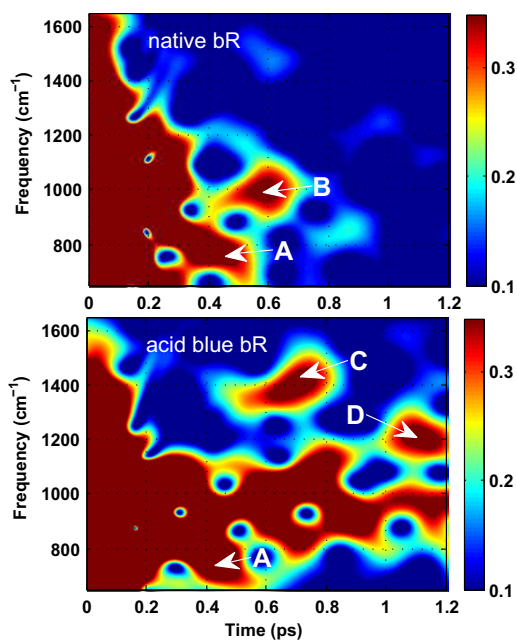| Mode ID	Frequency (cm^{-1})	Phase (°)	Decay time (fs)	Amplitude (relative)
N1	798	75	>2000	0.019
N2	841	−127	450	0.091
N3	901	94	570	0.098
N4	962	70	>2000	0.030
N5	989	−36	310	0.61
N6	1050	−133	570	0.18
N7	1173	143	>2000	0.047
N8	1330	−25	1130	0.19
N9	1382	−10	1000	0.22

FIGURE 2 Spectrogram of the interferogram of native and the acid blue bR sample with GaAs reference, based on sliding-window Fourier analysis with a Hann window of 400-fs length (200 fs FWHM). Arrows indicate regions of time-dependent frequencies (*A*) and recurrences (*B–D*).
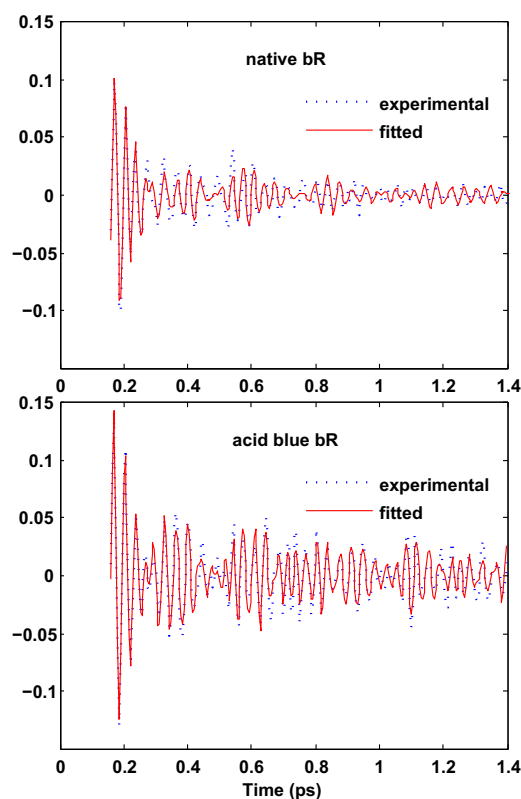

FIGURE 3 Vibrational part of the interferogram of the native sample fitted with seven vibrational modes, and the acid blue sample fitted with nine modes.

also shows the spectrogram taken from the IR emission of the acid blue form of bR that has a considerably longer-lived excited state (52,57). This sample provides more intense long-lived coherences (see also Fig. 3). In good correlation with the prolonged excited state, the lifetimes of the vibrational modes in the 800–1200 cm^{-1} region are markedly increased in this state. In addition, islandlike features appeared in regions C and D in Fig. 2. Since the structure of a spectrogram can depend highly on the sliding window applied, we repeated this analysis with shorter and longer window lengths. This inherently resulted in increased temporal and spectral resolution, respectively (see Fig. S2, Fig. S3, and Fig. S4), but did not affect the overall character of the spectrograms.

As an alternative and complementary way of analysis we fitted discrete damped vibrational modes to the interferogram, which made it possible to determine their amplitude, frequency, phase, and lifetime (see Materials and Methods for the detailed fitting procedure). The results of the fits are presented in Fig. 3 and Tables 1 and 2. The best results were obtained with seven modes for the native and nine for the acid blue sample. Although our own spectrograms, as well as previous studies from other laboratories (7,12, 32–34), indicated the occurrence of time-dependent frequencies of several modes, the large number of necessary free parameters precluded including this effect in the fitting model. For the same reason, the time evolution of the modes was modeled in the simplest way, supposing that the modes had an instant rise and a single exponential decay. The misfit

observable between 0.4 and 0.6 ps in the case of the native bR sample could be due, at least partially, to these limitations. In accordance with the overall tendency observed on the spectrograms (Fig. 2), the long-lived components are more pronounced in the acid blue sample than in native bR.

To validate the results of the fitting analysis in the frequency domain we calculated the power-spectrum estimation of the vibrational region of the interferograms and compared the results to those obtained from the fitting curves (Fig. 4). It is clear that all the significant peaks are modeled very well by the fitting procedure. The considerably higher amplitudes and narrower peaks in the case of acid blue bR again indicate more intense vibrations in this sample, with the dominance of long-lived modes. Otherwise, the general peak structure of the power spectrum corresponding to the two samples is similar, with two extra high-frequency peaks in the case of acid blue bR. The main tendency in the distribution of the peak intensities is determined by the spectral response of the measuring system (Fig. 4).

The good correlation between the measured and fitted curves in both the time (Fig. 3) and frequency (Fig. 4) domains raises the question to what extent the complex structure of the spectrograms in Fig. 2 can be reproduced by the applied fitting model. For this reason, the
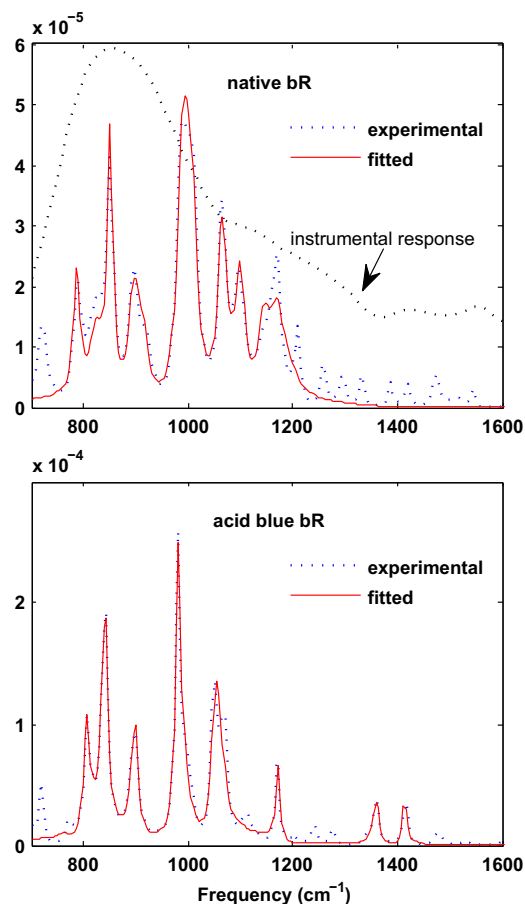
FIGURE 4   Power-spectrum estimates calculated from the experimental and fitted data for the vibrations from the native and acid blue bR samples in Fig. 3. Also indicated is the spectral response of the measuring system.
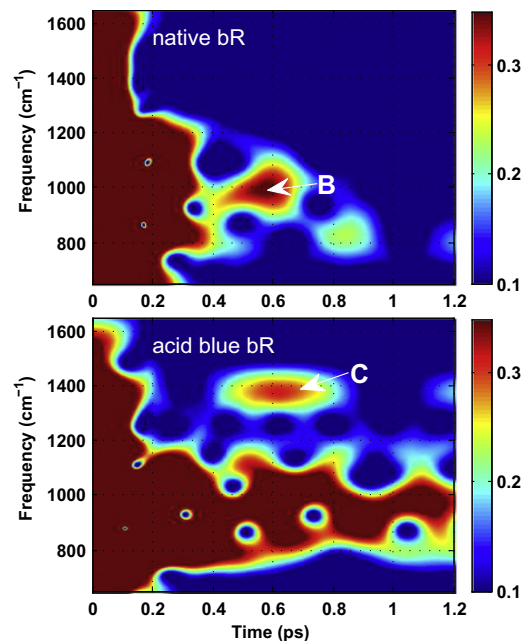

FIGURE 5   Spectrogram of the modeled interferogram fitted to the experimental data from the native and the acid blue sample with coloring identical to that on Fig. 2. The arrows mark regions where the recurrences are reproduced by the fit.

spectrograms of the fitting curves are presented in Fig. 5. For both the native and the acid blue sample, most features in the spectrograms of the measured data are observable on the simulated ones, including the isolated regions of high intensity (B and C). (Compare also the corresponding spectrograms in Fig. S2, Fig. S3, and Fig. S4.) This finding indicates that the apparent frequency recurrences, which are observed also on absorption kinetic data (12,32,33), should be handled with care. In our case, they may be the result of beating among modes of different frequencies. In particular, our calculation shows that the islandlike feature marked as region C in Fig. 5 can be well reproduced by taking into account only modes N8 and N9 in Table 2 (see Fig. S5). On the other hand, a similar structure in region D does not occur in the simulated spectrogram. Also, the simulated spectrograms do not reproduce the structures observable in region A of the two spectrograms in Fig. 2, indicating the presence of real time-dependent frequencies (7,12,33). In view of the long lifetime of the excited state in acid blue bR, we suggest that these features are due to anharmonic distortion of the excited-state PES.

DISCUSSION

In the following, we discuss our interpretation by addressing the assignment of the observed modes to molecular processes in light of numerous previous studies by both frequency domain spectroscopy (8–11,13,37,39–44) and ultrafast absorption and stimulated emission kinetics (7,12,28–34). According to the underlying theory (49), resonant excitation of the chromophore could induce vibrational coherences on both the electronically-excited- and ground-state PESs (in the latter case by a process similar to RISRS). Below, we attempt to assign the different modes to the excited and ground states of the resting form of bR and its J and K intermediates, mainly based on their lifetimes and the orientation of the vibrations.

Normal mode calculation is a common tool for assignment of modes obtained by conventional vibrational spectroscopy of bR (18,37,39). It was found that the position of the dominating lines observed by IR and resonance Raman measurements coincide very well with each other (38) and with the calculated modes (18,37). Our analysis is based on the resonance Raman spectra and calculated normal modes reported by Smith et al. (37), corresponding to the all-*trans* retinal in the resting state of bR. Strictly speaking, this allows only the assignment of vibrational coherences taking place on the S_0 PES. For the excited-state vibrations, one can expect some shift of the frequencies due to the high change in the bond configuration in the retinal backbone (19,24). However, to our knowledge no normal

mode calculation has been published for the S_1 state. The normal modes in the frequency range covered by our experimental method are HOOP wags (700–1000 cm^{-1}), C-C stretches (1100–1250 cm^{-1}), C-C-H in-plane rocks (1250–1400 cm^{-1}), lysine rocks, and different methyl-group and cyclohexene vibrations. The frequency of C=C stretches (1500–1600 cm^{-1}) and C=N stretch (1640 cm^{-1}) are beyond the observable region. The typical discrepancy between the frequencies of the calculated normal modes and the measured Raman peaks is 2–10 cm^{-1}, whereas the errors in the frequencies of the vibrational modes detected in this study (Tables 1 and 2) are somewhat higher. Within these uncertainties, the modes obtained from native bR (Table 1) can be at least partially correlated to the reported Raman peaks as follows.

Modes M2 and M4 (Table 1) correspond to the 852 cm^{-1} B_g mode and the A_u mode (985 cm^{-1}), respectively, of the HC$_7$=C$_8$H HOOP combination. M3 can be assigned to either the 881 cm^{-1}, 897 cm^{-1}, or 942 cm^{-1} Raman peak, or all of these, dominated by C$_{14}$H, C$_{10}$H, and NH HOOP wags, respectively. M5 is mapped to the 1048 cm^{-1} peak of the C$_{19}$ and C$_{20}$ out-of-plane methyl rocks. M7 can be assigned to any (or all) of the strong 1170 cm^{-1}, 1201 cm^{-1}, and 1214 cm^{-1} peaks dominated by C$_{10}$-C$_{11}$, C$_{14}$-C$_{15}$, and C$_8$-C$_9$ stretches, respectively. M1 and M6 cannot be clearly attributed to any reported Raman peak. It is interesting to note that these are the only modes listed in Table 1 that have lifetimes of >2 ps (see below). We stress that the HOOP modes are very weak in the resonance Raman spectrum of bR but are stronger than the C-C stretches in the coherent-emission experiments. We attribute this difference to indirect activation of the HOOP motions via coupling to directly activated stretching modes.

The dominant Raman peaks that do not give rise to strong peaks in the IR emission, although they fall in the observable region, are 830 cm^{-1} (lysine HOOP wag), 842 cm^{-1} (B_g mode of the HC$_{11}$=C$_{12}$H HOOP combination), 959 cm^{-1} (A_u mode of the previous combination), 1002 cm^{-1} (C$_{15}$H HOOP wag), and 1008 cm^{-1} (C$_{19}$ and C$_{20}$ symmetric in-plane methyl rocks). In addition, all in-plane H rocks, lysine rocks, symmetric in-plane and out-of-plane methyl deformations, and cyclohexene ring vibrations are missing.

The experimentally observed Raman spectrum of the acid blue form of bR shows minor differences with respect to the native one, mainly due to the existence of 13-*cis* retinal in this component (58). In accordance with the above assignments for native bR, we can correlate modes N3, N5, N6, and N7 of Table 2 with M3, M4, M5, and M7, respectively, of Table 1. Here, the missing HC$_{11}$=C$_{12}$H HOOP combination can be assigned to N2 (B_g mode at 842 cm^{-1}) and N4 (A_u mode at 959 cm^{-1}). The uncertainties in the mapping of modes M3 and M7 were found somewhat lowered for the acid blue sample; hence, N3 and N7 point more unequivocally to the Raman peaks at 897 cm^{-1} and 1170 cm^{-1}, respectively. N8 and N9 have no counterparts in Table 1.

N8 can be assigned to any of the four in-plane H rock modes between 1304 cm^{-1} and 1345 cm^{-1}. N9 could correspond either to the N-H in-plane mode at 1348 cm^{-1} or to the C$_{19}$ and C$_{20}$ symmetric methyl deformations at 1378 cm^{-1}.

There are also IR active modes that are not highly Raman active. This can be seen in incoherent IR emission spectra from free retinal and bR (59) that are due to hot ground states (60); these spectra show much stronger relative contributions from HOOP modes than do resonance Raman spectra, generally consistent with our coherent IR experiments. In particular, a relatively intense peak occurs at 768 cm^{-1}, close to our unidentified M1 mode. We note that it is difficult to make a direct comparison between the (cw) incoherent IR emission from the thermally populated ground state and our coherent IR emissions that are coupled to the optical activation and emanate primarily from the excited state (see below). In addition, as discussed below, the amplitudes of the modes observed by our second-order method depend highly also on the orientation of the vibration.

The spectrograms of the experimental traces (Fig. 2) show two main features not reproduced by the model calculation based on the fits with damped cosinusoidals starting at $t = 0$ (Fig. 5) (and hence not represented in Tables 1 and 2). A branch of diminishing frequencies is observable in region A of both spectrograms in Fig. 2. This frequency range corresponds to low-lying HOOP modes, with possible involvement of a lysine wag. The fact that this peninsula of vibrational activity cannot be modeled with the fits suggests that it reflects vibrations synchronized by the excitation pulse but set in motion in a delayed fashion. It is possible that (partial) isomerization of the retinal brings the direction of these vibrations into a favorable orientation for detection with our experimental arrangement (see below). In addition, in the spectrogram of the acid blue sample, an isolated peak takes place in region D that can be attributed to C-C stretches, but contributions from lysine or in-plane H rocks are also possible.

The striking dominance of the out-of-plane modes (mainly HOOP) over the in-plane modes (stretch) in the coherent IR emission is very interesting considering the geometrical properties of our experiment. The high-resolution atomic structure of bR (61) reveals that the plane of the all-*trans* retinal chromophore is almost completely perpendicular to that of the membrane, and the angle between its long axis and the membrane normal is ~69° (see also Fig. S6). Upon orientation, the arrangement of the retinal long axes takes a conical symmetry (Fig. S1), hence we detect macroscopically only the component of the motions in the direction of the membrane normal (46). Indeed, the observed C-C stretches have a component in this direction, as do the in-plane rocks, which, however, are completely missing from the detected modes of native bR. On the other hand, the dominating HOOP wags have only small components in the direction of the membrane normal. This observation indicates that the dominant part

of the emission does not originate from the planar resting structure of retinal. Rather, the majority of the coherent vibrational motions are born in transient nonplanar states related to the isomerization processes. In other words, we strongly suggest that the HOOP modes are coherently activated upon (partial) isomerization of the retinal on the timescale of ~200 fs.

According to recent QM/MM calculations, even in the resting state of bR, the $C_{13}=C_{14}$ bond is pretwisted by $20°$ (24). During the first 130 fs after the FC transition to S_1, the retinal remains in all-*trans* form, after which the torsion around the $C_{13}=C_{14}$ bond is started (25). The CI, corresponding to a seam of 60–90° $C_{13}=C_{14}$ dihedral angle is reached at ~200–450 fs (20,24,62), and the twisted conformation is maintained while the trajectory remains on the S_1 surface. After returning to S_0, the twisted conformation relaxes quickly to the planar form of either the all-*trans* or the 13-*cis* isomer, corresponding to the resting state of bR and its J intermediate, respectively. During the 90° twist, several HOOP wags get into observable positions for our experiment. In addition, detailed studies on the time evolution of all dihedral angles along the retinal backbone in visual rhodopsin (26,63) and bR (24,64) revealed that many of them change considerably in the vicinity of the FC transition and after reaching the CI, exciting HOOP-wag and in-plane-rock modes. The changing dihedral angles could considerably change the relative contribution of the in-plane and out-of-plane vibrational modes to the observed IR emission by increasing both the amplitude of the HOOP modes and their component in the membrane normal. The appearance of the $HC_{11}=C_{12}H$ HOOP combination in the acid blue sample, which was absent in the native one, is probably due to the deformation of the corresponding dihedral angle on excitation of a retinal population with a 13-*cis* conformation in its resting state.

Coherent oscillations observed on the red edge of the bR absorption band in transient absorption kinetics correspond to $C=C$ and C-C stretches and in-plane methyl rock modes (28,32) and were interpreted as ground-state coherences generated by the RISRS process (36). In contrast to this, a short-lived broad feature in the 850–950 cm^{-1} HOOP region appearing on the blue edge of the spectrum can be attributed to vibrational wave-packet motions on the potential surface of the excited state (32). This interpretation is consistent with that of the M2 and M3 modes obtained by our analysis; although the lifetimes are longer than in that case, they are still short enough to be interpreted as excited-state vibrational coherences. In a detailed study on time dependence of vibrational frequencies coupled to transient absorption kinetics, Kobayashi and co-workers reported the appearance of 900–1000 cm^{-1} HOOP modes in 30 fs after excitation to the FC state, together with coupled C-C stretching and C=C-H in-plane bending modes in the 1150–1250 cm^{-1} range (7,12,33,34). The frequencies of these modes mix in the interval of 150–200 fs, when retinal is highly nonplanar; subsequently, the original frequencies recover with highly weakened intensities. After 700 fs, the intensities of the C-C stretching and C=C-H in-plane bending modes recovered upon formation of the J intermediate. This scenario is consistent with the 230-fs and 260-fs decay times of our M3 and M4 HOOP modes, respectively, as well as the 410-fs decay time of M7, assigned as C-C stretching. On the other hand, no mode recovery after 700 fs is observable in our spectrogram (Fig. 2). We stress however, that our method detects all IR active vibrational modes activated directly or indirectly by optical excitation of the system, and—unlike in the case of the above studies—it is not dependent on coupling of the modes to the optical transitions of the ground, excited, and product states.

Dispersive line shapes observed in femtosecond stimulated Raman spectroscopy studies on bR (43) were analyzed in the framework of a process termed Raman initiated by nonlinear emission (RINE), resulting in vibrational coherences in the ground state. It was found that the RINE signal of the C=C, C-C, and methyl-rock modes decays in ~260 fs, which is significantly smaller than the lifetime of the S_1 electronic state. This was explained by an excited-state intramolecular vibrational redistribution (IVR) process: the initially FC-active modes relax by populating lower frequency modes, such as CCC bends, HOOP wags, and torsions, deforming the molecule toward the CI. Analysis of the dispersive lines using a recent, more complex alternative model of the same experimental data (65) with femtosecond stimulated Raman spectroscopy resulted in vibrational coherences of ~600-fs lifetime on the S_1 surface, roughly identical to the lifetime of S_1 itself. This indicates that vibrational coherences are not completely destroyed by IVR; they can be partially maintained even in a hot environment. Interpreting our M2, M3, M4, M5, and M7 modes, as well as the feature in region A of the spectrogram (Fig. 2), as excited-state vibrations would be consistent with that model. This interpretation is also supported by the prolonged overall decay of the IR emission from the acid blue sample (Figs. 2 and 3 and Table 2). In the absence of sufficient reference spectral information about this form of bR, a detailed analysis of its vibrational modes is out of the scope of this study. However, the marked correlation between the longer lifetime of the vibration and the slower and strongly biphasic decay of the excited state of the acid blue form (52,57) as compared to native bR indicates that the majority of the vibration motions we detect take place on the S_1 surface.

Due to their long decay time, the M1 (773 cm^{-1}) and M6 (1110 cm^{-1}) modes cannot be considered solely as excited-state vibrations. As stated earlier, these modes cannot be associated with any known Raman line of bR. Therefore, we do not assign them to pure bR ground-state coherences, but rather to vibrations that persist into the J state and/or the K state. Modes at corresponding frequencies were not

observed in transient Raman studies of the J state (8,10,11). Hence, we conclude that these motions are infrared-active but not (strongly) Raman-active; we note that the frequency range of <1100 cm^{-1} was not covered by transient IR absorption studies (13) of the J state. An alternative possibility is that these modes originate from a protein region near the chromophore and excited by the high dipole moment change taking place during and after the S_0-S_1 transition (19–24,46–48).

In conclusion, using the coherent infrared emission technique on oriented bR films, we were able to map the ensemble of infrared-active complex coherent motions of the retinal/protein complex. In the emission of native bR, we identified and characterized seven vibrational modes and a feature of time-dependent frequency. The majority of the modes were assigned as out-of-plane (HOOP or methyl) and one mode as C-C stretching, whereas two long-lived modes presumably persisting on the isomerization product states remain as yet unidentified. Based on different criteria, we deduce that (with the exception of the latter two modes) all modes belong to the potential surface of the S_1 electronic state. Note, however, that in principle, our experimental method may also generate ground-state vibrational coherences. A definitive mapping of the observed vibrational modes to the S_0 and S_1 electronic states requires two-dimensional difference frequency generation experiments (49). The existence of long-lived coherent out-of-plane vibrations during the complete time evolution of the excited state indicates that the isomerization process has a highly coherent nature, even in a hot environment. Since the applied detection method is uniquely sensitive to the orientation of these modes, their occurrence supports the idea that the isomerization involves large angular changes also in the vicinity of the C_{13}=C_{14} bond, in accordance with the double-bicycle-pedal model suggested by recent QM/MM calculations (24).

SUPPORTING MATERIAL

Six figures are available at http://www.biophysj.org/biophysj/supplemental/ S0006-3495(11)00199-8.

REFERENCES

1. Spudich, J. L., C. S. Yang, …, E. N. Spudich. 2000. Retinylidene proteins: structures and functions from archaea to humans. *Annu. Rev. Cell Dev. Biol.* 16:365–392.

2. Béjà, O., L. Aravind, …, E. F. DeLong. 2000. Bacterial rhodopsin: evidence for a new type of phototrophy in the sea. *Science.* 289: 1902–1906.

3. Haupts, U., J. Tittor, and D. Oesterhelt. 1999. Closing in on bacteriorhodopsin: progress in understanding the molecule. *Annu. Rev. Biophys. Biomol. Struct.* 28:367–399.

4. Lanyi, J. K. 2004. Bacteriorhodopsin. *Annu. Rev. Physiol.* 66:665–688.

5. Aharoni, A., B. Hou, …, Q. Zhong. 2001. Non-isomerizable artificial pigments: implications for the primary light-induced events in bacteriorhodopsin. *Biochemistry (Mosc.).* 66:1210–1219.

6. Abramczyk, H. 2004. Femtosecond primary events in bacteriorhodopsin and its retinal modified analogs: revision of commonly accepted interpretation of electronic spectra of transient intermediates in the bacteriorhodopsin photocycle. *J. Chem. Phys.* 120:11120–11132.

7. Kobayashi, T., A. Yabushita, …, M. Tsuda. 2007. Sub-5-fs real-time spectroscopy of transition states in bacteriorhodopsin during retinal isomerization. *Photochem. Photobiol.* 83:363–368.

8. Shim, S., J. Dasgupta, and R. A. Mathies. 2009. Femtosecond time-resolved stimulated Raman reveals the birth of bacteriorhodopsin's J and K intermediates. *J. Am. Chem. Soc.* 131:7592–7597.

9. Braiman, M., and R. Mathies. 1982. Resonance Raman spectra of bacteriorhodopsin's primary photoproduct: evidence for a distorted 13-*cis* retinal chromophore. *Proc. Natl. Acad. Sci. USA.* 79:403–407.

10. Doig, S. J., P. J. Reid, and R. A. Mathies. 1991. Picosecond time-resolved resonance Raman spectroscopy of bacteriorhodopsin's J, K, and KL intermediates. *J. Phys. Chem.* 95:6372–6379.

11. Atkinson, G. H., L. Ujj, and Y. D. Zhou. 2000. Vibrational spectrum of the J-625 intermediate in the room temperature bacteriorhodopsin photocycle. *J. Phys. Chem. A.* 104:4130–4139.

12. Kobayashi, T., T. Saito, and H. Ohtani. 2001. Real-time spectroscopy of transition states in bacteriorhodopsin during retinal isomerization. *Nature.* 414:531–534.

13. Herbst, J., K. Heyne, and R. Diller. 2002. Femtosecond infrared spectroscopy of bacteriorhodopsin chromophore isomerization. *Science.* 297:822–825.

14. Dobler, J., W. Zinth, …, D. Oesterhelt. 1988. Excited-state reaction dynamics of bacteriorhodopsin studied by femtosecond spectroscopy. *Chem. Phys. Lett.* 144:215–220.

15. Mathies, R. A., C. H. Brito Cruz, …, C. V. Shank. 1988. Direct observation of the femtosecond excited-state *cis-trans* isomerization in bacteriorhodopsin. *Science.* 240:777–779.

16. Levine, B. G., and T. J. Martínez. 2007. Isomerization through conical intersections. *Annu. Rev. Phys. Chem.* 58:613–634.

17. Robb, M. A., F. Bernardi, and M. Olivucci. 1995. Conical intersections as a mechanistic feature of organic photochemistry. *Pure Appl. Chem.* 67:783–789.

18. Garavelli, M., F. Negri, and M. Olivucci. 1999. Initial excited-state relaxation of the isolated 11-*cis* protonated Schiff base of retinal: evidence for in-plane motion from ab initio quantum chemical simulation of the resonance Raman spectrum. *J. Am. Chem. Soc.* 121: 1023–1029.

19. González-Luque, R., M. Garavelli, …, M. Olivucci. 2000. Computational evidence in favor of a two-state, two-mode model of the retinal chromophore photoisomerization. *Proc. Natl. Acad. Sci. USA.* 97: 9379–9384.

20. Molnar, F., M. Ben-Nun, …, K. Schulten. 2000. Characterization of a conical intersection between the ground and first excited state for a retinal analog. *J. Mol. Struct.* 506:169–178.

21. Salem, L., and P. Bruckmann. 1975. Conversion of a photon to an electrical signal by sudden polarisation in the N-retinylidene visual chromophore. *Nature.* 258:526–528.

22. Mathies, R., and L. Stryer. 1976. Retinal has a highly dipolar vertically excited singlet state: implications for vision. *Proc. Natl. Acad. Sci. USA.* 73:2169–2173.

23. Lewis, A. 1978. The molecular mechanism of excitation in visual transduction and bacteriorhodopsin. *Proc. Natl. Acad. Sci. USA.* 75: 549–553.

24. Altoè, P., A. Cembran, …, M. Garavelli. 2010. Aborted double bicycle-pedal isomerization with hydrogen bond breaking is the primary event of bacteriorhodopsin proton pumping. *Proc. Natl. Acad. Sci. USA.* 107:20172–20177.

25. Hayashi, S., E. Tajkhorshid, and K. Schulten. 2003. Molecular dynamics simulation of bacteriorhodopsin's photoisomerization using ab initio forces for the excited chromophore. *Biophys. J.* 85:1440–1449.

26. Hayashi, S., E. Tajkhorshid, and K. Schulten. 2009. Photochemical reaction dynamics of the primary event of vision studied by means of a hybrid molecular simulation. *Biophys. J.* 96:403–416.

27. Polli, D., P. Altoè, …, G. Cerullo. 2010. Conical intersection dynamics of the primary photoisomerization event in vision. *Nature.* 467: 440–443.

28. Dexheimer, S. L., Q. Wang, …, C. V. Shank. 1992. Femtosecond impulsive excitation of nonstationary vibrational states in bacteriorhodopsin. *Chem. Phys. Lett.* 188:61–66.

29. Bardeen, C. J., Q. Wang, and C. V. Shank. 1998. Femtosecond chirped pulse excitation of vibrational wave packets in LD690 and bacteriorhodopsin. *J. Phys. Chem. A.* 102:2759–2766.

30. Ye, T., E. Gershgoren, …, S. Ruhman. 1999. Resolving the primary dynamics of bacteriorhodopsin, and of a ′C-13=C-14 locked' analog, in the reactive excited state. *Chem. Phys. Lett.* 314:429–434.

31. Hou, B. X., N. Friedman, …, S. Ruhman. 2003. Comparing photoinduced vibrational coherences in bacteriorhodopsin and in native and locked retinal protonated Schiff bases. *Chem. Phys. Lett.* 381:549–555.

32. Kahan, A., O. Nahmias, …, S. Ruhman. 2007. Following photoinduced dynamics in bacteriorhodopsin with 7-fs impulsive vibrational spectroscopy. *J. Am. Chem. Soc.* 129:537–546.

33. Yabushita, A., and T. Kobayashi. 2009. Primary conformation change in bacteriorhodopsin on photoexcitation. *Biophys. J.* 96:1447–1461.

34. Yabushita, A., and T. Kobayashi. 2010. Vibrational fine structures revealed by the frequency-to-time fourier transform of the transient spectrum in bacteriorhodopsin. *J. Phys. Chem. B.* 114:4632–4636.

35. Chesnoy, J., and A. Mokhtari. 1988. Resonant impulsive-stimulated Raman scattering on malachite green. *Phys. Rev. A.* 38:3566–3576.

36. Pollard, W. T., S. L. Dexheimer, …, R. A. Mathies. 1992. Theory of dynamic absorption-spectroscopy of nonstationary states. 4. Application to 12-fs resonant impulsive Raman spectroscopy of bacteriorhodopsin. *J. Phys. Chem.* 96:6147–6158.

37. Smith, S. O., M. S. Braiman, …, R. A. Mathies. 1987. Vibrational analysis of the all-*trans*-retinal chromophore in light-adapted bacteriorhodopsin. *J. Am. Chem. Soc.* 109:3108–3125.

38. Bagley, K., G. Dollinger, …, L. Zimányi. 1982. Fourier transform infrared difference spectroscopy of bacteriorhodopsin and its photoproducts. *Proc. Natl. Acad. Sci. USA.* 79:4972–4976.

39. Gerwert, K., and F. Siebert. 1986. Evidence for light-induced 13-*cis*, 14-s-*cis* isomerization in bacteriorhodopsin obtained by FTIR difference spectroscopy using isotopically labelled retinals. *EMBO J.* 5: 805–811.

40. Song, L., and M. A. El-Sayed. 1998. Primary step in bacteriorhodopsin photosynthesis: bond stretch rather than angle twist of its retinal excited-state structure. *J. Am. Chem. Soc.* 120:8889–8890.

41. Terentis, A. C., L. Ujj, …, G. H. Atkinson. 2005. Primary events in the bacteriorhodopsin photocycle: torsional vibrational dephasing in the first excited electronic state. *Chem. Phys.* 313:51–62.

42. Andresen, E. R., and P. Hamm. 2009. Site-specific difference 2D-IR spectroscopy of bacteriorhodopsin. *J. Phys. Chem. B.* 113:6520–6527.

43. McCamant, D. W., P. Kukura, and R. A. Mathies. 2005. Femtosecond stimulated Raman study of excited-state evolution in bacteriorhodopsin. *J. Phys. Chem. B.* 109:10449–10457.

44. Gross, R., C. Schumann, …, M. Sheves. 2009. Ultrafast protein conformational alterations in bacteriorhodopsin and its locked analogue BR5.12. *J. Phys. Chem. B.* 113:7851–7860.

45. Groot, M. L., M. H. Vos, …, J. L. Martin. 2002. Coherent infrared emission from myoglobin crystals: an electric field measurement. *Proc. Natl. Acad. Sci. USA.* 99:1323–1328.

46. Groma, G. I., A. Colonna, …, J. L. Martin. 2004. Resonant optical rectification in bacteriorhodopsin. *Proc. Natl. Acad. Sci. USA.* 101: 7971–7975.

47. Colonna, A., G. I. Groma, …, M. H. Vos. 2007. Quantification of sudden light-induced polarization in bacteriorhodopsin by optical rectification. *J. Phys. Chem. B.* 111:2707–2710.

48. Groma, G. I., J. Hebling, …, E. Riedle. 2008. Terahertz radiation from bacteriorhodopsin reveals correlated primary electron and proton transfer processes. *Proc. Natl. Acad. Sci. USA.* 105:6888–6893.

49. Venkatramani, R., and S. Mukamel. 2005. Dephasing-induced vibronic resonances in difference frequency generation spectroscopy. *J. Phys. Chem. B.* 109:8132–8143.

50. Oesterhelt, D., and W. Stoeckenius. 1974. Isolation of the cell membrane of *Halobacterium halobium* and its fractionation into red and purple membrane. *Methods Enzymol.* 31(Pt A):667–678.

51. Váró, G., and L. Keszthelyi. 1983. Photoelectric signals from dried oriented purple membranes of *Halobacterium halobium. Biophys. J.* 43:47–51.

52. Colonna, A., G. I. Groma, and M. H. Vos. 2005. Retinal isomerization dynamics in dry bacteriorhodopsin films. *Chem. Phys. Lett.* 415:69–73.

53. Váró, G., and J. K. Lanyi. 1989. Photoreactions of bacteriorhodopsin at acid pH. *Biophys. J.* 56:1143–1151.

54. Groma, G. I., L. Kelemen, …, G. Váró. 2001. Photocycle of dried acid purple form of bacteriorhodopsin. *Biophys. J.* 81:3432–3441.

55. Oppenheim, A. V., R. W. Schafer, and J. R. Buck. 1999. Discrete-Time Signal Processing. Prentice Hall, Upper Saddle River, NJ.

56. Stoica, P., and R. L. Moses. 1997. Introduction to Spectral Analysis. Prentice Hall, Upper Saddle River, NJ.

57. Logunov, S. L., M. A. El-Sayed, …, J. K. Lanyi. 1996. Photoisomerization quantum yield and apparent energy content of the K intermediate in the photocycles of bacteriorhodopsin, its mutants D85N, R82Q, and D212N, and deionized blue bacteriorhodopsin. *J. Phys. Chem.* 100:2391–2398.

58. Massig, G., M. Stockburger, and T. Alshuth. 1985. Structure of bacteriorhodopsin in the acidified membrane and at high ionic-strength - resonance Raman-study. *Can. J. Chem.* 63:2012–2017.

59. Gagarinov, A. G., O. V. Degtyareva, …, E. L. Terpugov. 2006. Stimulated infrared emission in all-trans retinal and wild-type bacteriorhodopsin under CW optical pumping: studies by FT-IR spectroscopy. *Vib. Spectrosc.* 42:231–238.

60. Wang, J. P., and M. A. El-Sayed. 2002. Time-resolved long-lived infrared emission from bacteriorhodopsin during its photocycle. *Biophys. J.* 83:1589–1594.

61. Luecke, H., B. Schobert, …, J. K. Lanyi. 1999. Structure of bacteriorhodopsin at 1.55 Å resolution. *J. Mol. Biol.* 291:899–911.

62. Garavelli, M., P. Celani, …, M. Olivucci. 1997. The $C_5H_6NH_2^+$ protonated Shiff base: an ab initio minimal model for retinal photoisomerization. *J. Am. Chem. Soc.* 119:6891–6901.

63. Frutos, L. M., T. Andruniów, …, M. Olivucci. 2007. Tracking the excited-state time evolution of the visual pigment with multiconfigurational quantum chemistry. *Proc. Natl. Acad. Sci. USA.* 104:7764–7769.

64. Warshel, A., and Z. Chu. 2001. Nature of the surface crossing process in bacteriorhodopsin: computer simulations of the quantum dynamics of the primary photochemical event. *J. Phys. Chem. B.* 105:9857–9871.

65. Niu, K., B. Zhao, …, S. Y. Lee. 2010. Analysis of femtosecond stimulated Raman spectroscopy of excited-state evolution in bacteriorhodopsin. *J. Chem. Phys.* 132:084510.